JNS

CLINICAL ARTICLE

Computational fluid dynamic analysis of the initiation of cerebral aneurysms

Soichiro Fujimura, PhD,[1,2] Kazutoshi Tanaka, MS,[2] Hiroyuki Takao, MD, PhD,[2–4] Takuma Okudaira, MS,[2] Hirokazu Koseki, MD,[3] Akiko Hasebe, MD,[6] Takashi Suzuki, PhD,[2,5] Yuya Uchiyama, MS,[2,4] Toshihiro Ishibashi, MD,[3] Katharina Otani, PhD,[3,5] Kostadin Karagiozov, MD, PhD,[3] Koji Fukudome, PhD,[1] Motoharu Hayakawa, MD,[6] Makoto Yamamoto, PhD,[1] and Yuichi Murayama, MD[3]

[1]Department of Mechanical Engineering, Tokyo University of Science; Departments of [2]Innovation for Medical Information Technology and [3]Neurosurgery, The Jikei University School of Medicine; [4]Graduate School of Mechanical Engineering, Tokyo University of Science; [5]Siemens Healthcare K. K., Tokyo; and [6]Department of Neurosurgery, Fujita Health University, Aichi, Japan

OBJECTIVE Relationships between aneurysm initiation and hemodynamic factors remain unclear since de novo aneurysms are rarely observed. Most previous computational fluid dynamics (CFD) studies have used artificially reproduced vessel geometries before aneurysm initiation for analysis. In this study, the authors investigated the hemodynamic factors related to aneurysm initiation by using angiographic images in patients with cerebral aneurysms taken before and after an aneurysm formation.

METHODS The authors identified 10 cases of de novo aneurysms in patients who underwent follow-up examinations for existing cerebral aneurysms located at a different vessel. The authors then reconstructed the vessel geometry from the images that were taken before aneurysm initiation. In addition, 34 arterial locations without aneurysms were selected as control cases. Hemodynamic parameters acting on the arterial walls were calculated by CFD analysis.

RESULTS In all de novo cases, the aneurysmal initiation area corresponded to the highest wall shear stress divergence (WSSD point), which indicated that there was a strong tensile force on the arterial wall at the initiation area. The other previously reported parameters did not show such correlations. Additionally, the pressure loss coefficient (PLc) was statistically significantly higher in the de novo cases ($p < 0.01$). The blood flow impact on the bifurcation apex, or the secondary flow accompanied by vortices, resulted in high tensile forces and high total pressure loss acting on the vessel wall.

CONCLUSIONS Aneurysm initiation may be more likely in an area where both tensile forces acting on the vessel wall and total pressure loss are large.

https://thejns.org/doi/abs/10.3171/2021.8.JNS211452

KEYWORDS cerebral aneurysm; de novo aneurysm; computational fluid dynamics; hemodynamics; vascular disorders

Most unruptured aneurysms are detected incidentally by MRI or CT screening for diseases other than aneurysms. As the prevalence of cerebral aneurysms has been reported to be much higher than that of their clinical presentation, the evaluation of aneurysm initiation in cases that were already treated or were symptomatic is not expected to reflect the real random pathogenetic mechanisms.[1–6] If we can understand the mechanism of aneurysm initiation by examining the de novo initiation process after having confirmed and investigated the preceding normal arterial condition, we may be able to predict and eventually prevent aneurysms. Currently, however, it is very difficult to predict aneurysm initiation by obtaining angiographic images before initiation and then being able to follow that patient.

Aneurysm initiation is considered to be related to chronic inflammation in the cerebrovascular wall.[7,8] According to previous research, chronic inflammation may be caused by hemodynamic effects on the arterial wall in addition to other clinical factors such as smoking history,

ABBREVIATIONS ACA = anterior cerebral artery; AComA = anterior communicating artery; BA = basilar artery; CFD = computational fluid dynamics; D_{in} = equivalent diameter at the inlet of the analysis domain; GON = gradient oscillatory number; ICA = internal carotid artery; MCA = middle cerebral artery; OSI = oscillatory shear index; PLc = pressure loss coefficient; VA = vertebral artery; WSS = wall shear stress; WSSD = WSS divergence; WSSG = WSS gradient.

SUBMITTED June 14, 2021. **ACCEPTED** August 9, 2021.
INCLUDE WHEN CITING Published online December 21, 2021; DOI: 10.3171/2021.8.JNS211452.

alcohol consumption, hypertension, decreased estrogen levels, or dental bacterial infection.[3,8–12] Computational fluid dynamics (CFD) analysis allows evaluation of the relationships between hemodynamic forces on the arterial wall and aneurysm initiation. Previous studies reported that the wall shear stress (WSS), which is the frictional force on the arterial wall produced by blood flow; the oscillatory shear index (OSI), which measures the directional changes of WSS during cardiac cycles, the WSS gradient (WSSG) and the gradient oscillatory number (GON), were key factors to aneurysmal initiation.[13–21] To reveal the relationships between hemodynamics and aneurysm initiation, CFD analysis for the cerebral arteries before aneurysm initiation is essential. However, in most studies, the CFD analyses were performed on artificially reproduced states of vessel geometry before aneurysm initiation, created by manually removing the aneurysm from the images that were taken after an aneurysm was completely developed.[15,17,18] Some CFD research has focused on de novo cases or blister aneurysm formation using the vessel geometry before aneurysm initiation, but these are a very limited number of cases because angiographic images before aneurysm initiation are rarely obtained within normal diagnostic protocols.[13,14,19,20] To the best of our knowledge, 3 analyzed cases using images before the aneurysm has initiated have been published.[14,19,20]

In the present study, we analyzed hemodynamics using CFD on 10 de novo aneurysms on angiographic images acquired before the aneurysms initiated. We also conducted CFD analysis on 34 arterial locations (10 control individuals) on an arterial geometry without aneurysm initiation. The parameter for evaluating tensile and compressive stress called wall shear stress divergence (WSSD) as well as previously reported hemodynamic parameters related to aneurysmal initiation was applied.[22] These parameters were compared between de novo and control cases. Our objective was to qualitatively and quantitatively investigate hemodynamic factors related to aneurysm initiation. Here we report the application of CFD analysis based on images obtained before actual aneurysm initiation in a de novo case series.

Methods

Patient Selection and Clinical Data

This study was approved by the local ethics committees at our institutions and was conducted in accordance with the Declaration of Helsinki. We retrieved clinical and radiological data from January 2003 to December 2018 of de novo aneurysms that were subsequently identified during follow-up imaging in treated or "under observation" patients from the databases of three institutions. We identified 16 patients with de novo aneurysms detected after a period of up to 8 years from the initial negative study at a location where no aneurysm was present. We performed CFD analysis of the 3D angiographic imaging data taken before aneurysmal initiation. We excluded 6 patients due to absent 3D image data or inadequate image quality for CFD analysis, for which main arteries were not connected to each other or high noise level was present due to artifacts. Finally, 10 aneurysms in 10 patients were collected, and we defined them as de novo. Their sites were the internal carotid artery (ICA), middle cerebral artery (MCA), anterior cerebral artery (ACA), basilar artery (BA), and vertebral artery (VA). To compare the hemodynamic differences between cases with and without de novo aneurysm initiation, we also identified 10 patients who had no aneurysms in the anterior or posterior circulation but had multiple aneurysms in the "opposite" posterior or anterior circulations (not of interest), respectively, and classified them as control patients. Additionally, these selected control patients had unruptured aneurysms, longer follow-up periods, and an older average age than the de novo patients. According to these criteria, control patients were extracted randomly and confirmed by two blinded neurosurgeons, who reviewed each of the 24 locations (in 5 patients) without aneurysms in the anterior circulation (anterior control) and 10 locations (in 5 patients) without aneurysms in the posterior circulation (posterior control) (Table 1). For the same reasons as for de novo patients, control patients for whom adequate 3D images were not available were excluded. For these patients the oldest 3D imaging data during the follow-up term were used for the CFD analysis. In addition, the clinical information, including sex, history of alcohol consumption, history of smoking, hyperlipidemia, and hypertension were included.

CFD Analysis

Arterial Geometry Generation

The modeled regions for anterior and posterior circulation ranged from the petrous portion of the ICA petrous to the A_2 ACA and M_2 MCA segments, and from the V_4 VA segment to the terminal branch of the BA. Based on the generated model, the size of the de novo aneurysms was measured in 3D (the neck length is the maximum diameter at the neck plane and the height is the maximum height from the center of the neck plane). The detailed method is included in the Supplemental Material.

Computational Conditions

Both computational unstructured volumetric grid generation and CFD analysis were performed on the generated STL data according to settings of previous studies using STAR-CCM+ (v10.06.010) multiphysics CFD software (Siemens PLM software).[20,23] In anterior circulation cases, the inlet pulsatile conditions were imposed according to the mass flow rate at the ICA determined in healthy adult volunteers and measured by Ford et al.[24] On the other hand, in posterior circulation cases one-third of the ICA flow rate was imposed at the VA.[24] We assumed static pressure of 0 Pa at all outlets. The detailed method is included in the Supplemental Material.

Analysis Domain

We defined the analysis domain for comparison of the hemodynamic parameters among the cases. In the case of a specific bifurcation type, such as bifurcations of the MCA, ACA–anterior communicating artery (AComA), terminal BA, and VA union, the domain was defined by planes set 5 mm distally and proximally to the bifurcation point, respectively. In the case of an ICA sidewall type, the

TABLE 1. Statistical difference between de novo and control cases for clinical data and hemodynamic parameters

Parameter	De Novo (pts: n = 10; analyzed cases: n = 10)	Control (pts: n = 10; analyzed cases: n = 34)	p Value
Clinical data			
Analyzed location, cases			0.761
ICA	3 (30.0%)	10 (29.4%)	
MCA	2 (20.0%)	10 (29.4%)	
ACA	3 (30.0%)	4 (11.8%)	
BA	1 (10.0%)	5 (14.7%)	
VA	1 (10.0%)	5 (14.7%)	
Size of de novo, mm			
Height	2.9 ± 0.5	—	—
Neck length	4.1 ± 0.7	—	—
Ruptured aneurysms	1 (10.0%)	0 (0%)	1.000
No. of aneurysms	2.4 ± 0.8	2 ± 0	0.149
Pt data			
Age at de novo diagnosis, yrs	61.4 ± 7.2	—	—
Age at analysis, yrs	56.1 ± 8.3	73.1 ± 8.69	**<0.01**
Follow-up duration, yrs	4.8 ± 3.1	8.9 ± 0.32	**<0.01**
Male sex	3 (30.0%)	4 (40.0%)	1.000
Alcohol	1 (10%)	0 (0%)	1.000
Smoking	3 (30%)	3 (30%)	1.000
Hyperlipidemia	2 (20%)	0 (0%)	0.474
Hypertension	2 (20%)	6 (60%)	0.170
Hemodynamic parameters			
WSSD*	$1.54 \times 10^{-2} \pm 1.25 \times 10^{-2}$	$7.84 \times 10^{-3} \pm 1.88 \times 10^{-2}$	0.261
WSS*	$1.25 \times 10^{-1} \pm 4.30 \times 10^{-2}$	$1.38 \times 10^{-1} \pm 2.07 \times 10^{-1}$	0.238
WSSG*	$3.74 \times 10^{-1} \pm 1.44 \times 10^{-1}$	$3.26 \times 10^{-1} \pm 1.58 \times 10^{-1}$	0.273
OSI	$7.04 \times 10^{-3} \pm 5.68 \times 10^{-3}$	$4.35 \times 10^{-3} \pm 1.83 \times 10^{-3}$	0.399
GON	$3.37 \times 10^{-2} \pm 2.06 \times 10^{-2}$	$2.45 \times 10^{-2} \pm 8.08 \times 10^{-3}$	0.238
Pressure*	$3.53 \times 10^{1} \pm 1.98 \times 10^{1}$	$2.44 \times 10^{1} \pm 1.22 \times 10^{1}$	0.121
Vorticity*	7.10 ± 2.15	6.08 ± 1.16	0.216
PLc	2.98 ± 0.46	2.06 ± 0.67	**<0.01**

Pt = patient.
Values are presented as number (%) of patients or mean ± SD unless otherwise indicated. Boldface type indicates statistical significance.
* Normalized value.

proximal plane was set 1 mm proximally to the ophthalmic artery and the distal plane was set 1 mm proximally to the MCA-ACA bifurcation point to cover the ICA C_1 and C_2 segments, since all ICA de novo cases were included in this area. For de novo patients, the analysis domain was only set at initiation sites. On the other hand, for control patients, the analysis domains were set at locations in the anterior circulation (ICA, MCA bifurcation, and ACA-AComA) and in the posterior circulation (BA terminal and VA union) that did not initiate aneurysms (i.e., the hemodynamic parameters were extracted from up to 5 sites [the right and left ICA, MCA bifurcations, and ACA-AComA] in every control patient with analyzed anterior circulation and from up to 2 sites [BA terminal and VA union] in every control patient with analyzed posterior circulation). As a result, 34 control noninitiation sites in 10 patients were analyzed (Table 1).

Hemodynamic Parameters

After the CFD analysis was performed, we calculated hemodynamic parameters which were previously reported in the study of aneurysmal initiation, growth, and rupture, including WSS, WSSG, OSI, GON, pressure, and pressure loss coefficient (PLc).[25–27] In addition, to evaluate tensile and compressive stress on the vascular wall, we introduced the parameter WSS divergence (WSSD), which was originally developed to estimate the risk of aneurysm rupture.[22] Vorticity was also evaluated to compare the complexity of the flows inside the arteries. In this study, parameters such as WSS, WSSG, WSSD, pressure, and vorticity were normalized by dynamic pressure, equivalent diameter at the inlet of the analysis domain (D_{in}), or velocity at the inlet of analysis domain to compare values among the cases[20,26] (in this report normalized parameters are marked with asterisk). Time-dependent parameters were averaged over

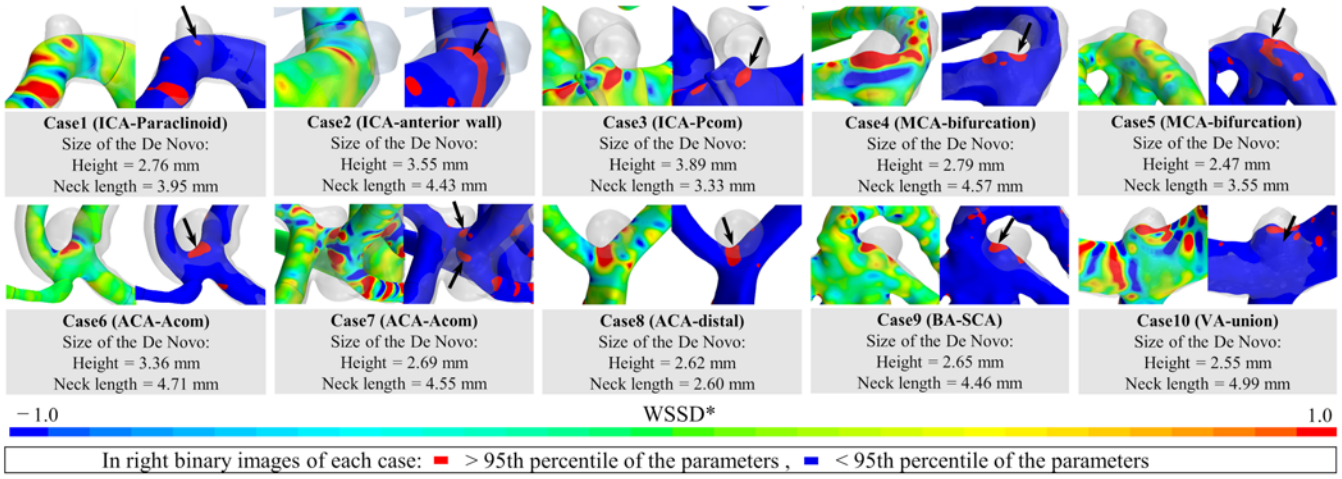

FIG. 1. Qualitative correspondence between CFD result (WSSD*) and initiation area for all analyzed de novo cases. The *semi-transparent silver areas* are aneurysms after they have grown. The *normal color contour images* are placed in left of each case. In right binary images of each case, the *red area* indicates where the parameter values are over the 95th percentile in the analysis domain, and the *blue area* indicates when they are under the 95th percentile. The *black arrows* are added if the initiation area and high-value (*red area*) area correspond. Location, height, and neck length of each de novo aneurysm are also shown.

the last cardiac cycle. The detailed definition of the parameters is included in the Supplemental Material.

Statistical Analysis

Clinical and hemodynamic parameters were compared between the de novo and control groups. Fisher's exact test was used for nominal variables. The Kolmogorov-Smirnov test was used to test whether the continuous variables, including hemodynamic parameters, of the de novo and control groups followed a normal distribution. The Mann-Whitney U-test was used if either group did not show normal distribution. If both groups exhibited normal distribution, either Student's t-test or Welch's t-test was used according to the presence or nonpresence of equal variance, respectively. A p value less than 0.05 was considered statistically significant. All statistical analyses were performed using SAS 9.4 (SAS Institute, Inc.).

Results

Clinical Characteristics of De Novo Aneurysms and Controls

Details of the differences between de novo and control cases are summarized in Table 1. Although all images of the de novo cases for CFD analysis were taken before aneurysmal initiation, in one of the de novo cases the aneurysm was ruptured (i.e., the de novo aneurysm was identified after the subarachnoid hemorrhage). The mean age of the patients was 61.4 ± 7.2 years when they were diagnosed with a de novo aneurysm. Since we used the image before the de novo aneurysm initiation to conduct CFD analysis, the mean age of the de novo patients at the CFD analysis point was 56.1 ± 8.3 years. The average follow-up period of the de novo patients, which is the period from the date of the initial 3D imaging study to the date of de novo aneurysm diagnosis, was 4.8 ± 3.1 years. On the other hand, the control patients were statistically significantly older (73.1 ± 8.7 years) and had a longer follow-up period (8.9 ± 0.3 years) than the de novo patients, since we preselected the follow-up to be longer and patients were older than the averages for the de novo patients. The average dimensions of de novo aneurysms were 2.9 ± 0.5 mm (height) and 4.1 ± 0.7 mm (neck length).

Hemodynamic Forces on the Arterial Wall and Aneurysmal Initiation Area

We qualitatively observed the relationship between hemodynamic forces on the arterial wall and aneurysmal initiation area. The calculated hemodynamic parameters, including WSSD*, WSS*, WSSG*, OSI, GON, and pressure* are illustrated for each de novo case in Fig. 1 and Supplementary Fig. 1. In these figures, in addition to the normal color contour images, binary images with red and blue demonstrate the hemodynamic parameters. The binary images were defined based on the parameter value: the red area is the high-value, with parameter values over the 95th percentile in the analysis domain, and the blue area parameter values are under the 95th percentile. Additionally, the figures also include the aneurysms after their initiation, which is illustrated using a semitransparent silver color merged into each illustration. The figures contain a black arrow if the three blinded neurosurgeons agreed to the correspondence between the initiation area and the high-value area (red area). This result did not show qualitative correspondence between the aneurysm initiation area location and the regions with high-value hemodynamic parameters—WSS*, WSSG*, OSI, GON, and pressure*—that have been reported as key factors of aneurysm initiation in previous studies. The correspondence rates were 70%, 80%, 40%, 20%, and 60% for WSS*, WSSG*, OSI, GON, and pressure*, respectively (see Supplementary Fig. 1). On the other hand, the newly introduced hemodynamic parameter, WSSD*, showed 100% correspondence to the aneurysmal initiation area (a high WSSD* area was ob-

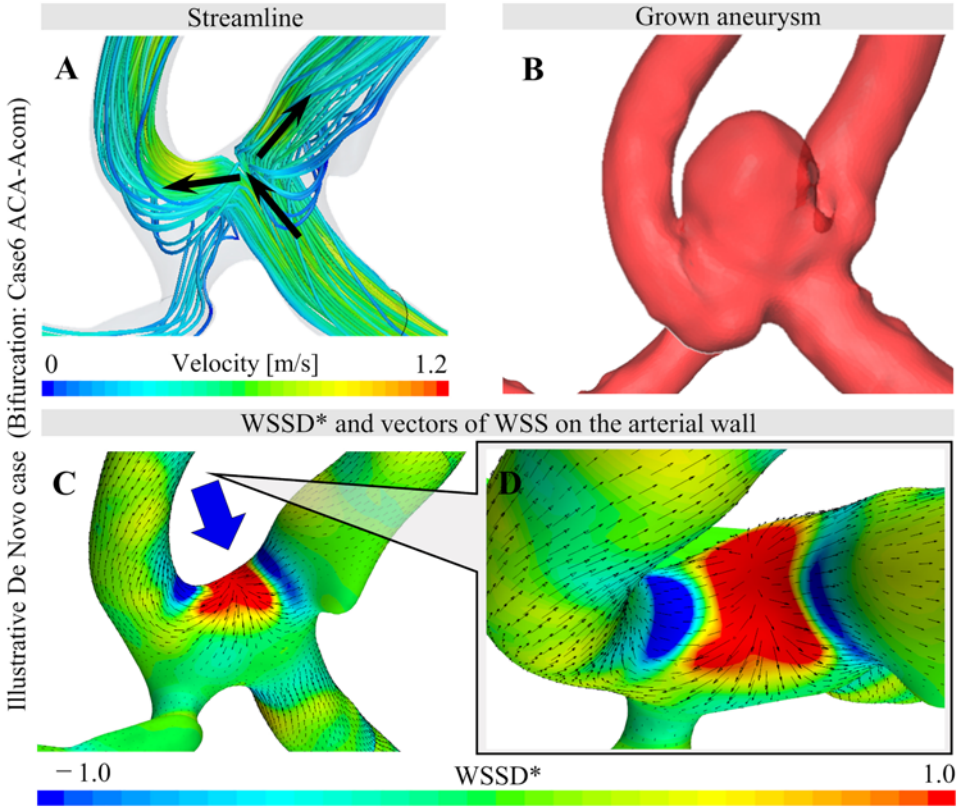

FIG. 2. Illustrative de novo case at a bifurcation. **A:** Streamlines before the aneurysm has grown. The *black arrows* indicate the main flow. **B:** Geometry of grown aneurysm. **C:** WSSD distribution on vessels before aneurysm has initiated. The *thin black arrows* indicate the vector of wall shear stress. **D:** WSSD viewed in the direction of the *blue arrow*.

served at every initiation area) (see Fig. 1). In addition, illustrative cases of de novo aneurysms at a bifurcation and on a sidewall are shown in Figs. 2 and 3 with their streamlines and WSSDs* along with their respective aneurysms, initiated afterwards. In Figs. 2C and D and 3D and E, the WSS vectors represented by thin black arrows are also displayed. The thick black arrows in Figs. 2A and 3A show the flow direction. In the case of the sidewall aneurysm, streamlines were displayed in two directions: from outside of the siphon curve (Fig. 3A) and from inside of the siphon curve using a blue wide arrow to show direction (Fig. 3B). We observed that the inward flow separated from the main flow, passing the bend, and generated a secondary flow inside the bend, which is circled by a white line in Fig. 3B. Illustrative cases of control at a bifurcation and on a sidewall are also shown in Supplementary Fig. 2 with their streamlines and WSSD*.

Hemodynamic Differences Between De Novo Aneurysms and Control Locations

Details of the hemodynamic differences between de novo and control cases are summarized in Table 1. Although the qualitative observation results showed good correspondence between high WSSD* positions and aneurysmal initiation area, the values of the parameter did not show statistically significant differences as were shown for the other hemodynamic parameters except PLc. PLc was statistically significantly higher in de novo cases, which indicates that total pressure loss in the analysis domain was larger in these cases than in controls. The averaged values for vorticity, PLc, and equivalent diameter at the inlet of the analysis domain (D_{in}) values, were also summarized for each location in Table 2. Since there were too few de novo cases to perform statistical tests when analyzing at each location, the differences of the parameters between de novo and control cases were summarized.

Discussion

Relationship Between Hemodynamic Factors and Aneurysmal Initiation

Previous investigators have conducted CFD analysis to clarify the hemodynamic factors associated with aneurysm initiation. Meng et al. hypothesized that aneurysm initiation occurred with destructive remodeling from the combination of high WSS and high WSSG.[28,29] The OSI, which was introduced by Ku et al. as a parameter resulting from the relationship between blood flow and atherosclerosis, has also been used to report values related to aneurysm initiation.[15,18,20,21,30] Shimogonya et al. also proposed GON as a way to quantify the hemodynamic tension/compression forces.[16] However, in some of the previous studies, the arterial geometry was reproduced artificially by manually removing the aneurysm from the images that

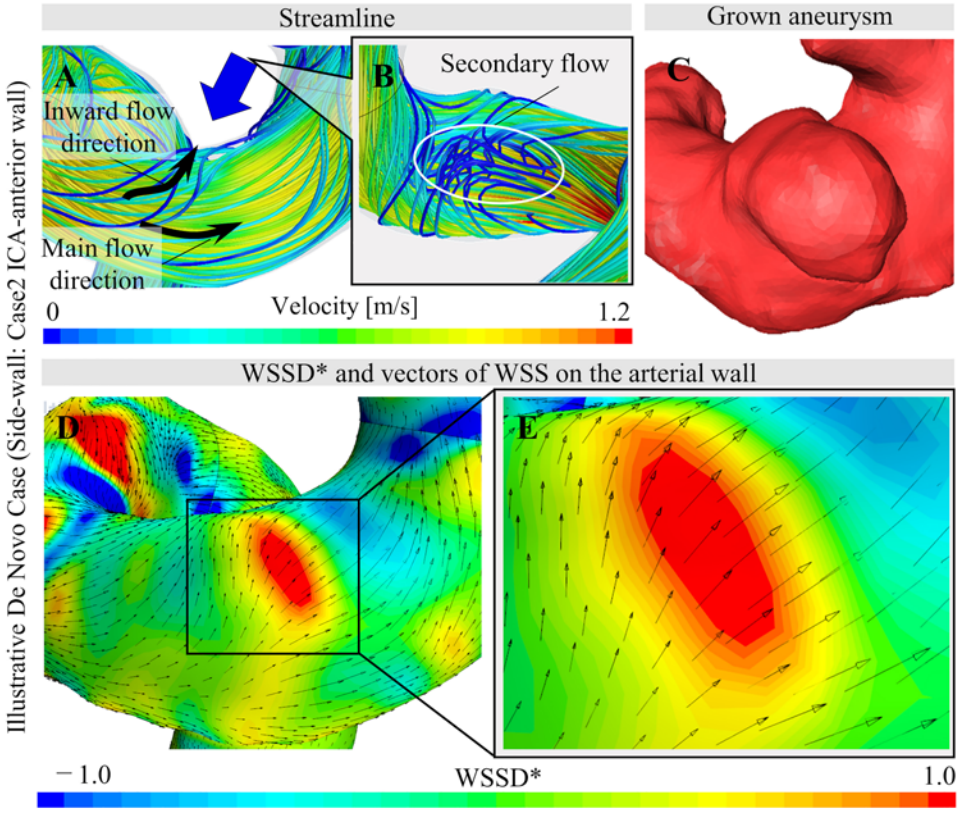

FIG. 3. Illustrative de novo case of a sidewall type aneurysm. **A:** Streamlines before the aneurysm has grown. The *black arrows* indicate the main flow. **B:** Streamlines viewed in the direction of the *blue arrow*. Secondary flow is circled with a *white line*. **C:** Geometry of the grown aneurysm. **D:** WSSD distribution on vessels before aneurysm initiation. The thin *black arrows* indicate the vector of wall shear stress. **E:** WSSD at the *circled region* where the inward flow separated from the main flow.

contained aneurysms.[15,17,18] It is highly probable that the artificially reproduced vessel geometry did not accurately represent the state before aneurysm initiation. Since the results of CFD analysis highly depend on vessel geometry, the correct hemodynamic characteristics before aneurysmal initiation might have not been obtained with the use of artificially reproduced vessel geometry. Therefore, it is obviously appropriate to use the arterial geometry before the aneurysm has initiated for proper investigation of aneurysmal initiation. The main problem of such a study design is the difficulty in collecting a substantial number of cases. Although Kulcsár et al. examined the hemodynamics related to aneurysm initiation at certain arterial segments that later initiated an aneurysm, these authors analyzed only 3 cases.[14] Shojima et al. and Tanaka et al. also conducted CFD analysis on 3 patients in whom aneurysms were initiated during follow-up.[19,20] Thus, until now it has been difficult to effectively use CFD analysis to fully evaluate the hemodynamic features involved in aneurysmal initiation.

Hemodynamic Characteristics Involved in De Novo Cases Compared to Controls

In this study, we performed CFD analysis in 10 de novo aneurysm cases, which is to our knowledge the largest number investigated until now. Our results indicated that the aneurysm initiation areas did not have good correspondence to the locations of high values for hemodynamic parameters that have been previously reported, such as WSS*, OSI, WSSG*, and GON.[13–21] On the other hand, it was confirmed that the location of high WSSD*, which has not been consistently reported as a key parameter for aneurysmal initiation, had very good correspondence to the aneurysmal initiation areas in all cases. WSSD* represents the tensile and compressive stress on the vessel wall due to hemodynamic effects. In other words, the location where the blood flow produced high tensile forces matched the aneurysmal initiation areas. Although statistically significant differences were not observed between de novo and control cases for the values of WSSD*, the differences were greater in de novo cases (the average WSSD* values of de novo and control cases were $1.54 \times 10^{-2} \pm 1.25 \times 10^{-2}$ and $7.84 \times 10^{-3} \pm 1.88 \times 10^{-2}$, respectively). Koseki et al. demonstrated real-time wall motion of the prospective location of an intracranial aneurysm using a rat model and indicated that mechanical stretching promotes macrophage migration via activation of adventitial fibroblasts followed by expression of chemoattractant protein. Thus, these authors hypothesized that mechanical stretching may be one of the most essential triggers for aneurysm initiation. This report also supports our findings that high tensile force may cause aneurysm initiation.[31] On the other

TABLE 2. Average values of vorticity, PLc, and D_{in}

Parameters	De Novo	Control	Difference
Anterior circulation			
ICA	(n = 3)	(n = 10)	
Vorticity*	9.17 ± 0.68	6.36 ± 1.39	44.2%
PLc	2.79 ± 0.33	1.86 ± 0.69	49.8%
D_{in}, mm	4.02 ± 0.76	4.44 ± 0.35	–9.37%
MCA	(n = 2)	(n = 10)	
Vorticity*	5.74 ± 1.96	5.61 ± 0.88	2.22%
PLc	2.93 ± 0.74	1.70 ± 0.38	72.5%
D_{in}, mm	$3.08 \pm 5.24 \times 10^{-3}$	3.33 ± 0.25	–7.59%
ACA	(n = 3)	(n = 4)	
Vorticity*	6.48 ± 2.17	6.85 ± 0.42	–5.42%
PLc	3.31 ± 1.65	2.60 ± 0.93	27.4%
D_{in}, mm	2.94 ± 0.47	3.37 ± 0.42	–12.7%
Posterior circulation			
BA	(n = 1)	(n = 5)	
Vorticity*	4.24	5.22±0.72	–18.7%
PLc	2.30	2.42 ± 0.43	–5.00%
D_{in}, mm	3.98	4.49 ± 0.30	–11.3%
VA	(n = 1)	(n = 5)	
Vorticity*	8.30	7.00 ± 0.95	18.5%
PLc	3.36	2.17 ± 0.78	54.5%
D_{in}, mm	4.85	5.15 ± 0.38	–5.77%

* Normalized value.

hand, a statistically significant difference between de novo and control cases was observed for PLc, which indicates that the total pressure loss in the analysis domain was significantly larger for de novo cases. Takao et al. and Suzuki et al. concluded that PLc has a significant effect on aneurysm rupture from the results of CFD analysis for ruptured and unruptured aneurysms during observation.[25,26] They also concluded that hemodynamic stability denoted by low PLc reduces the natural vessel wall resistance to hemodynamic changes such as rapid blood pressure elevation, thereby increasing rupture risk. Additionally, they hypothesized that the "remodeling process" might be the transformation of vessel geometry in order to avoid artery wall interference of blood flow, and as a result, PLc eventually changed from high to low during aneurysm development. Our present results are consistent with this hypothesis, and we can consider aneurysmal initiation as a remodeling process that has occurred in the high-PLc region. Our results imply that an aneurysm may initiate in the area where both tensile forces acting on vessel wall and total pressure loss are high. These findings may suggest some future methodological application using CFD to assess the potential risk of aneurysm initiation at certain sites even before an aneurysm is detectable. To validate the CFD methodology as a risk assessment tool, a large prospective cohort study will be needed as well as solutions to the issues that are mentioned in the *Study Limitations* section.

Reason for Observation of High WSSD and High PLc in Bifurcation and Sidewall De Novo Cases

The reason why high WSSD and high PLc were observed in de novo cases may depend on whether the initiation area was at a bifurcation, such as ACA-AComA, MCA, or BA terminal, or at a sidewall, such as an ICA siphon. In the case of a bifurcation, the blood flow impact on the bifurcation apex causes increased total pressure loss that results in a higher PLc. In addition, blood flow spread due to the collision at the apex generates a tensile force to stretch the vessel wall. In the illustrative de novo case of a bifurcation aneurysm, the blood flow collision occurred at the apex of the bifurcation, resulting in a spread of the flow, as shown in Fig. 2A, and WSSD became high at the collision point due to the spread WSS vector (see Fig. 2C and D), which induced the aneurysm to initiate from that exact point (see Fig. 2B). Meanwhile, the diameter of the parent artery was measured at the inlet plane of the analysis domain as D_{in} for each case, as shown in Table 2. When we focused on the results for bifurcations (MCA, ACA, BA, VA), we confirmed that D_{in} was smaller in de novo than in control cases (5.77% to 12.7%). These results imply that concentrated dense flow produced by the small parent artery diameter also contributes to high WSSD and high PLc on the arterial wall.

In the case of sidewall aneurysms, we considered that the divergence flow and secondary flow accompanied by vortices resulted in high tensile forces acting on the vessel wall and high total pressure loss. Our results confirmed that the curvature of the siphon causes secondary flow, in which part of the blood flow goes inside around the bending wall of the artery as shown in Fig. 3A with the black arrow. The high WSSD* was present at the divergence point where the blood flow separates into an inward flow direction and a main flow direction (see Fig. 3D and E). Moreover, the total pressure loss denoted by PLc increased because the main flow path was narrowed due to secondary flow vortex formation inside the bend (see Fig. 3B). Comparing the vorticity* between de novo and control cases of ICA, the value was 44.2% higher in the de novo cases, as shown in Table 2. These observations on vortices are further supported by Csippa et al., who presented a case with strong secondary flow patterns at the site of a future aneurysm.[32] Riccardello et al. also concluded that secondary flow patterns may play a major role in the initiation of side-wall aneurysm initiation.[33]

Study Limitations

This study has several potential limitations. Due to the small sample size of de novo cases, statistical tests could not be performed when analyzing at each location separately. Regarding the CFD analysis, the use of a rigid wall, Newtonian blood model, and non–patient-specific boundary conditions were the main limitation of this study. However, some previous studies have reported that our analysis methods were useful ways for understanding the hemodynamic characteristics of the endovascular arterial environment.[34,35] Li et al. also reported that patient-specific inflow boundary conditions may not be necessary for making predictions using CFD because the same hemodynamic parameters showed statistically

significant differences regardless of the use of patient-specific or generalized inflow boundary conditions.[36] The patient angiographical image data were obtained from CTA, except for 1 patient with MRA data in the de novo case group. Although the exception is for only 1 case, the nonstandardized imaging modality is one of the limitations in CFD analysis since this difference may influence the values of hemodynamic parameters. For control cases, it was considered that no aneurysms would be initiated afterward. However, we have no absolute certainty for this assumption. To reduce the effect of this limitation, we selected control cases indicating a higher risk of aneurysm initiation than the de novo cases (i.e., control case patients had multiple aneurysms in the circulation not used as a control [anterior or posterior], longer follow-up periods, and older age than the de novo cases). Although the analysis domains were defined based on the anatomical findings in ICA cases, or 5-mm length from the bifurcation point at the other sites, the domain definition may vary based on the CFD operators. In addition, it remains unclear whether influences of factors other than the hemodynamic, such as genetic predisposition or inflammation or factors from the patient's clinical condition, accelerate the aneurysm initiation process or not. Though aneurysm growth is suggested to be relevant to chronic inflammation, the process of initiation remains to be elucidated. Although the hemodynamic parameters that we present could be factors associated with aneurysm initiation, we need further research to address these limitations, taking into consideration animal experimental aneurysm models. Finally, whether the high parameter value position corresponded to the site of the aneurysmal initiation area is largely determined by the observer's arbitrary judgement. Therefore, we used multiple blinded observers. To reduce the effect of these limitations, a multicenter study of a larger cohort should be considered in the future.

Conclusions

To investigate the hemodynamic factors related to aneurysmal initiation, we analyzed blood flow in 10 de novo and 34 control arterial sites using CFD. In all de novo cases, the aneurysmal initiation area corresponded to the high WSSD* point, which indicated that the tensile force strongly affected the arterial wall. Another hemodynamic parameter, PLc, which indicates the total pressure loss in the arteries, was statistically significantly higher in de novo cases. The high WSSD* and high PLc were caused by blood flow collision or the existence of secondary flow. These results imply that an aneurysm initiates in a region where both tensile forces acting on the vessel wall and total pressure loss are high. The measurement of these parameters may help in predicting aneurysmal initiation based on CFD analysis.

Acknowledgments

Dr. Fujimura was supported by JSPS KAKENHI grant number JP20J30001.

References

1. Ferns SP, Sprengers ME, van Rooij WJ, van den Berg R, Velthuis BK, de Kort GA, et al. De novo aneurysm formation and growth of untreated aneurysms: a 5-year MRA follow-up in a large cohort of patients with coiled aneurysms and review of the literature. *Stroke*. 2011;42(2):313-318.
2. Wermer MJ, van der Schaaf IC, Velthuis BK, Algra A, Buskens E, Rinkel GJ. Follow-up screening after subarachnoid haemorrhage: frequency and determinants of new aneurysms and enlargement of existing aneurysms. *Brain*. 2005; 128(Pt 10):2421-2429.
3. Juvela S, Poussa K, Porras M. Factors affecting formation and growth of intracranial aneurysms: a long-term follow-up study. *Stroke*. 2001;32(2):485-491.
4. David CA, Vishteh AG, Spetzler RF, Lemole M, Lawton MT, Partovi S. Late angiographic follow-up review of surgically treated aneurysms. *J Neurosurg*. 1999;91(3):396-401.
5. Tsutsumi K, Ueki K, Morita A, Usui M, Kirino T. Risk of aneurysm recurrence in patients with clipped cerebral aneurysms: results of long-term follow-up angiography. *Stroke*. 2001;32(5):1191-1194.
6. Sprengers ME, van Rooij WJ, Sluzewski M, Rinkel GJ, Velthuis BK, de Kort GA, Majoie CB. MR angiography follow-up 5 years after coiling: frequency of new aneurysms and enlargement of untreated aneurysms. *AJNR Am J Neuroradiol*. 2009;30(2):303-307.
7. Chyatte D, Bruno G, Desai S, Todor DR. Inflammation and intracranial aneurysms. *Neurosurgery*. 1999;45(5):1137-1147.
8. Kataoka H. Molecular mechanisms of the formation and progression of intracranial aneurysms. *Neurol Med Chir (Tokyo)*. 2015;55(3):214-229.
9. Francis SE, Tu J, Qian Y, Avolio AP. A combination of genetic, molecular and haemodynamic risk factors contributes to the formation, enlargement and rupture of brain aneurysms. *J Clin Neurosci*. 2013;20(7):912-918.
10. Starke RM, Thompson JW, Ali MS, Pascale CL, Martinez Lege A, Ding D, et al. Cigarette smoke initiates oxidative stress-induced cellular phenotypic modulation leading to cerebral aneurysm pathogenesis. *Arterioscler Thromb Vasc Biol*. 2018;38(3):610-621.
11. Vlak MH, Rinkel GJ, Greebe P, Algra A. Risk of rupture of an intracranial aneurysm based on patient characteristics: a case-control study. *Stroke*. 2013;44(5):1256-1259.
12. Pyysalo MJ, Pyysalo LM, Pessi T, Karhunen PJ, Öhman JE. The connection between ruptured cerebral aneurysms and odontogenic bacteria. *J Neurol Neurosurg Psychiatry*. 2013; 84(11):1214-1218.
13. Kono K, Masuo O, Nakao N, Meng H. De novo cerebral aneurysm formation associated with proximal stenosis. *Neurosurgery*. 2013;73(6):E1080-E1090.
14. Kulcsár Z, Ugron A, Marosfoi M, Berentei Z, Paál G, Szikora I. Hemodynamics of cerebral aneurysm initiation: the role of wall shear stress and spatial wall shear stress gradient. *AJNR Am J Neuroradiol*. 2011;32(3):587-594.
15. Singh PK, Marzo A, Howard B, Rufenacht DA, Bijlenga P, Frangi AF, et al. Effects of smoking and hypertension on wall shear stress and oscillatory shear index at the site of intracranial aneurysm formation. *Clin Neurol Neurosurg*. 2010; 112(4):306-313.
16. Shimogonya Y, Ishikawa T, Imai Y, Matsuki N, Yamaguchi T. Can temporal fluctuation in spatial wall shear stress gradient initiate a cerebral aneurysm? A proposed novel hemodynamic index, the gradient oscillatory number (GON). *J Biomech*. 2009;42(4):550-554.
17. Geers AJ, Morales HG, Larrabide I, Butakoff C, Bijlenga P, Frangi AF. Wall shear stress at the initiation site of cerebral aneurysms. *Biomech Model Mechanobiol*. 2017;16(1):97-115.
18. Sunderland K, Jiang J. Multivariate analysis of hemodynamic parameters on intracranial aneurysm initiation of the internal carotid artery. *Med Eng Phys*. 2019;74:129-136.
19. Shojima M, Nemoto S, Morita A, Oshima M, Watanabe E,

Saito N. Role of shear stress in the blister formation of cerebral aneurysms. *Neurosurgery*. 2010;67(5):1268-1275.
20. Tanaka K, Takao H, Suzuki T, Fujimura S, Uchiyama Y, Otani K, et al. Relationship between hemodynamic parameters and cerebral aneurysm initiation. *Annu Int Conf IEEE Eng Med Biol Soc*. 2018;2018:1347-1350.
21. Watanabe T, Isoda H, Takehara Y, Terada M, Naito T, Kosugi T, et al. Hemodynamic vascular biomarkers for initiation of paraclinoid internal carotid artery aneurysms using patient-specific computational fluid dynamic simulation based on magnetic resonance imaging. *Neuroradiology*. 2018;60(5):545-555.
22. Zhang Y, Takao H, Murayama Y, Qian Y. Propose a wall shear stress divergence to estimate the risks of intracranial aneurysm rupture. *ScientificWorldJournal*. 2013;2013:508131.
23. Hoi Y, Woodward SH, Kim M, Taulbee DB, Meng H. Validation of CFD simulations of cerebral aneurysms with implication of geometric variations. *J Biomech Eng*. 2006;128(6):844-851.
24. Ford MD, Alperin N, Lee SH, Holdsworth DW, Steinman DA. Characterization of volumetric flow rate waveforms in the normal internal carotid and vertebral arteries. *Physiol Meas*. 2005;26(4):477-488.
25. Takao H, Murayama Y, Otsuka S, Qian Y, Mohamed A, Masuda S, et al. Hemodynamic differences between unruptured and ruptured intracranial aneurysms during observation. *Stroke*. 2012;43(5):1436-1439.
26. Suzuki T, Takao H, Rapaka S, Fujimura S, Ioan Nita C, Uchiyama Y, et al. Rupture risk of small unruptured intracranial aneurysms in Japanese adults. *Stroke*. 2020;51(2):641-643.
27. Suzuki T, Stapleton CJ, Koch MJ, Tanaka K, Fujimura S, Suzuki T, et al. Decreased wall shear stress at high-pressure areas predicts the rupture point in ruptured intracranial aneurysms. *J Neurosurg*. 2019;132(4):1116-1122.
28. Meng H, Swartz DD, Wang Z, Hoi Y, Kolega J, Metaxa EM, et al. A model system for mapping vascular responses to complex hemodynamics at arterial bifurcations in vivo. *Neurosurgery*. 2006;59(5):1094-1101.
29. Meng H, Wang Z, Hoi Y, Gao L, Metaxa E, Swartz DD, Kolega J. Complex hemodynamics at the apex of an arterial bifurcation induces vascular remodeling resembling cerebral aneurysm initiation. *Stroke*. 2007;38(6):1924-1931.
30. Ku DN, Giddens DP, Zarins CK, Glagov S. Pulsatile flow and atherosclerosis in the human carotid bifurcation. Positive correlation between plaque location and low oscillating shear stress. *Arteriosclerosis*. 1985;5(3):293-302.
31. Koseki H, Miyata H, Shimo S, Ohno N, Mifune K, Shimano K, et al. Two diverse hemodynamic forces, a mechanical stretch and a high wall shear stress, determine intracranial aneurysm formation. *Transl Stroke Res*. 2020;11(1):80-92.
32. Csippa B, Závodszky G, Paál G, Szikora I. A new hypothesis on the role of vessel topology in cerebral aneurysm initiation. *Comput Biol Med*. 2018;103:244-251.
33. Riccardello GJ Jr, Changa AR, Al-Mufti F, Singh IP, Gandhi C, Roman M, Prestigiacomo CJ. Hemodynamic impingement and the initiation of intracranial side-wall aneurysms. *Interv Neuroradiol*. 2018;24(3):288-296.
34. Chung B, Cebral JR. CFD for evaluation and treatment planning of aneurysms: review of proposed clinical uses and their challenges. *Ann Biomed Eng*. 2015;43(1):122-138.
35. Xiang J, Tutino VM, Snyder KV, Meng H. CFD: computational fluid dynamics or confounding factor dissemination? The role of hemodynamics in intracranial aneurysm rupture risk assessment. *AJNR Am J Neuroradiol*. 2014;35(10):1849-1857.
36. Li W, Wang S, Tian Z, Zhu W, Zhang Y, Zhang Y, et al. Discrimination of intracranial aneurysm rupture status: patient-specific inflow boundary may not be a must-have condition in hemodynamic simulations. *Neuroradiology*. 2020;62(11):1485-1495.

Disclosures

T. Suzuki and K. Otani are full-time employees of Siemens Healthcare.

Author Contributions

Conception and design: Fujimura, Takao. Acquisition of data: Fujimura, Tanaka, Takao, Okudaira, Hasebe, Hayakawa. Analysis and interpretation of data: Fujimura, Tanaka. Drafting the article: Fujimura. Critically revising the article: Murayama, Fujimura, Okudaira, Koseki, Otani, Karagiozov. Reviewed submitted version of manuscript: all authors. Statistical analysis: Fujimura, Tanaka. Administrative/technical/material support: Murayama, Fujimura, Fukudome, Yamamoto. Study supervision: Murayama, Takao, Ishibashi, Fukudome, Hayakawa, Yamamoto.

Supplemental Information

Online-Only Content

Supplemental material is available with the online version of the article.

Supplemental Material. https://thejns.org/doi/suppl/10.3171/2021.8.JNS211452.

Correspondence

Yuichi Murayama: The Jikei University School of Medicine, Tokyo, Japan. ymurayama@jikei.ac.jp.